

ARChEaN: Aerodynamics of Rotors in Confined ENvironments Study in Ground and Corner Effect

S. Prothin, C. Fernandez Escudero, T. Jardin, and N. Doué
ISAE-Supaero, Université de Toulouse, France

ABSTRACT

The work presented in this paper is part of a project called ARChEaN (Aerodynamic of Rotors in Confined Environment) whose objective is to study the interactions of a micro-drone rotor with its surroundings in the case of flight in enclosed environments such as those encountered, for example, in archaeological exploration of caves. To do so the influence of the environment (walls, ground, ceiling...) on the rotor's aerodynamic performance as well as on the flow field between the rotor and the surroundings will be studied. This paper will focus in two different configurations: flight near the ground and flight near a corner (wall and ground) and the results will be analysed and compared to a general case consisting of flight far away from any obstacle. In order to carry out this analysis both a numerical and an experimental approach will be carried out in parallel. The objective is to validate the numerical model with the results obtained experimentally and to benefit from the advantages of both approaches. This research work is an important step as it will lead to knowledge on how to operate these systems as to minimise the possible negative environment disturbances, reduce fuel consumption and predict the micro drone's behaviour during its enclosed flights.

1 INTRODUCTION

Since their first developments, drones (unpiloted aircrafts) have revolutionised flight as we know it, opening a wide range of new possibilities which were unconceivable some decades ago. Drones allow us to go further than ever and their applications, which go from military uses to observation, exploration, meteorology, audio-visuals etc., are nowadays growing exponentially in parallel to new technological developments. Their versatility and flexibility make them a great sector in which to carry out new research and development projects.

The study focuses on how a micro rotor of a drone at stationary flight interacts with its environment. This will lead to improving the efficiency of this type of drone and to reducing the effects of detrimental phenomena on the local environment. The aerodynamic forces experienced by the micro rotor will be measured and the velocity and pressure distribution in the fluid surrounding it will be evaluated. The analysis and comprehension of this phenomenon will allow us to create models that represent the physics involved in these situations to integrate them in the drone's control laws.

The idea of this paper is to carry out new configuration cases and to study them using both a numerical and an experimental approach in parallel in order to compare the two of them and to benefit from the advantages that each one has to offer.

In this document, the context of the study will be explained, the two study approaches presented in order to explain and analyse the results obtained with each one and, finally the two will be compared. A list of nomenclature and a list the figures presented as well as the bibliography studied is included at the end in order to aid the reader in his/her understanding of this text.

In this project it was found that very few previous investigations had been carried out regarding the aerodynamics of micro-drone flight in closed environments which means, on one hand, that any results found will be of great interest as it is a very new study field with many applications but, at the same time that not much guidance is available. Regarding the out of ground effect (OGE) and the in ground effect (IGE), the first study cases of this study; there have been a significant number of studies carried out. However, the vast majority consider helicopter flight which means that the results are valid for large Reynolds number and since this project involves drones, small Reynolds numbers and since this project involves drones, small Reynolds numbers are involved so the results of these investigations do not necessarily apply. Furthermore, no studies have been found regarding flight in corner effect.

Although the complete list of bibliographical references consulted during the development of this project are presented at the end of this paper.

2 GEOMETRY AND CONFIGURATIONS

2.1 Rotor geometry

As previously explained, two approaches will be carried out in the present project. An experimental approach will be made in order to encounter the real phenomena and, additionally, CFD simulations will be developed to achieve a more thorough knowledge of the aerodynamics

involved. The two approaches will be constantly compared and validated with one another.

The geometry of rotor selected for every test carried out in this project is a two-blade rotor with rectangular blades of 100mm in length and 25mm in chord (c), having an aspect ratio (AR) of 4. As the [figure 1](#) shows, the radius of the rotor (R) is 125mm. Similarly, this rotor geometry will be reproduced in the numerical simulations. The blades have a constant angle of attack of 15 degrees.

2.2 Confined configurations

A closed environment is complicated to simulate as it includes many variables regarding the types of obstacles encountered, the distances between the obstacles from each other and from the drone etc. In order to simplify the problem and be able to study the phenomena in a general way, different study cases have been chosen to simulate different enclosed configurations. Since the ARChEaN project started in 2014 various configurations have been tested before arriving to the configurations analyzed throughout this report. In [figure 2](#), all these configurations will be briefly listed and explained.

- **Off ground effect (OGE):** the reference case without obstacles.
- **In Ground Effect (IGE):** presence of a wall downstream of the rotor.
- **In Ceiling Effect (ICE):** presence of a wall upstream of the rotor.
- **In Wall Effect (IWE):** presence of a wall perpendicular to the rotor plane.
- **In Channel Effect (ICHE):** presence of two walls, one upstream and the other downstream of the rotor.
- **In Low Corner Effect (ILoCE):** presence of two walls, one downstream of the rotor and the other perpendicular to the rotor plane.
- **In Upper Corner Effect (IUpCE):** presence of two walls, one upstream of the rotor and the other perpendicular to the rotor plane.

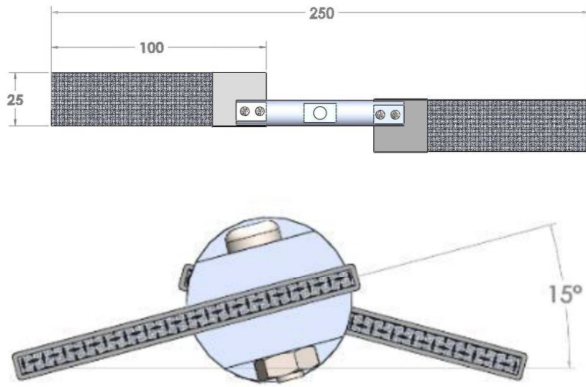


Figure 1 – Rotor geometry

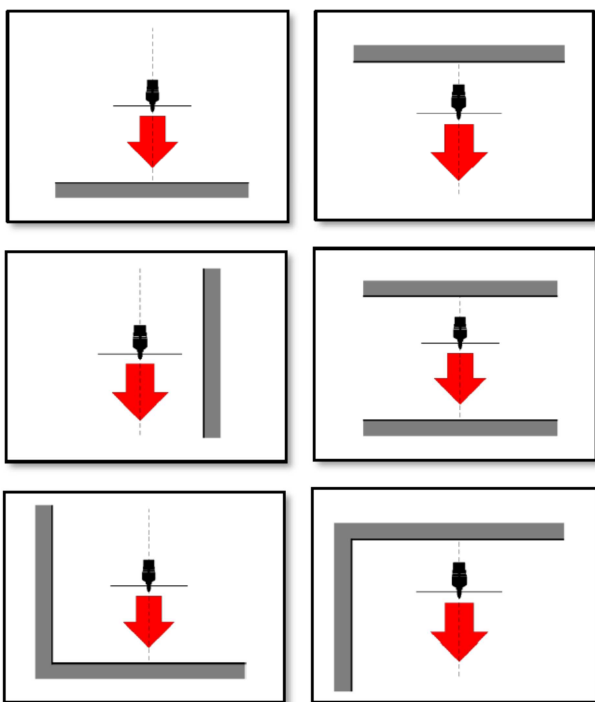


Figure 2 – Wall's configurations

In this paper we will present only ILoCE, cases (OGE, IGE, ICE, IChE) were studied and presented in [16].

The configuration studied here is the in low corner effect (ILoCE) which, similarly, refers to the particularities encountered by an aircraft when it is flying or hovering close to the ground or over a flat surface and close to a perpendicular wall or flat surface simultaneously. Again, every test and simulation was conducted in hovering flight conditions.

Within this configuration, three different cases will be analysed each with a different rotor to ground and rotor to wall distance. To characterise each case the dimensionless magnitude h/R , previously explained in the IGE configuration will be used, and we will introduce a new dimensionless magnitude, d/R where d is the distance from the centre of the rotor to the wall and R , again, is the rotor length.

The cases studied within this configuration will therefore be referred to as:

- ILoCE $h/R=2$ $d/R=2$
- ILoCE $h/R=2$ $d/R=3$
- ILoCE $h/R=3$ $d/R=2$

Similarly to in the IGE configuration, the objective is to fly at a constant lift value of 2N. Therefore, experimental tests on each of these configurations will also be carried out to obtain the rotation speeds required which will then be imposed in the numerical simulations, validated and used to obtain the blade effort distribution and the behaviour of the fluid around the rotor. Additionally, in the ILoCE case, further experimental analysis of the wake will be carried out using PIV (particle image velocimetry) measurements. Further information on both the numerical and experimental approaches will be detailed in the corresponding sections further on.

3 EXPERIMENTAL APPROACH

3.1 Efforts measurements

As mentioned before, all the configurations in this paper have been carried out considering a constant value of the total lift of 2N. The rotation speed corresponding to this lift value changes significantly depending on the configuration studied. These speeds have therefore been obtained experimentally. The apparatus used to obtain the experimental values plays a crucial role in the results obtained. Therefore, the main

components will be explained as well as their importance in the experiment.

The rotor frame of reference is shown below to help understand the setup. The balance has a different frame of reference as will be explained further on but the measurements will be converted to rotor frame of reference since the results will be expressed as seen by the rotor, [figure 3](#).

It is the main measurement tool which allows the forces and moments in three directions to be measured. The balance, showed in [figure 4](#), has a cylindrical shape. It is 21.6mm long and has a diameter of 25 mm. This balance is a non-intrusive object since it doesn't cause any perturbation to the flow field due to its perfect integration in the experimental setup. The sensing range of the balance is 125N for the forces along the X and Y axis, 500N along the Z axis and 3Nm for each moment. The maximum error in a measurement given by the manufacturer, and verified in our laboratory, is of 1 % in force and 1.25 % in torque.

A 350W brushless motor, the MikroKopter® MK3638, is connected to the rotor providing it with the necessary power for rotation.

To simulate the presence of the ground we use a table. This table of measurements is composed of nine PMMA detachable plates of 30 by 30cm constituting a 90 by 90 cm surface. Similarly a wall made out of a single piece is placed perpendicularly to it to simulate the wall.

To place the rotor at different distances we use a displacement system. A steel support rod was used to join the displacement system and the motor ensemble. The data of each measurement point was acquired at constant rotational and static conditions reproducing rotor hovering. Four different measurements were done for each set velocity-position to verify the measurement's repeatability. During the tests, the blade's

azimuthal position was acquired and the atmospheric conditions (T_{atm} , P_{atm}) measured.

The convergence of signal-spectrums for every variable is checked. If the correct convergence is showed, the mean of the 50000 samples is calculated for every parameter.

3.2 PIV measurements

As previously mentioned in the geometry and configuration section, a PIV analysis will be carried out to achieve an experimental knowledge of the behaviour of the fluid surrounding the rotor in the ILoCE cases.

For each ILoCE case the rotor plane of symmetry, which is perpendicular to the ground and to the wall, will be analyzed as well as other planes parallel to it to obtain a 3d velocity distribution of the fluid volume centered around the rotor, [figure 5](#).

The tracer particles chosen for this experiment were olive oil particles (mean diameter of 1 micron) produced by a generator TOPAS ATM 210 H. The mixing of the particles has been carried out in the whole closed room where the experiments took place before the acquisition phase to ensure the flow near the rotor was not being affected.

The laser used in these tests is the DualPower Bernouilli PIV 200-15. It is a pulse laser with double cavity which emits light at 532 nm with a cadence of up to 2 x 15 Hz. It delivers an energy pulse of 2 x 200mJ which is spread into a layer with the help of a cylindrical lens. For the acquisition of two consecutive double images each cavity emits a pulse with a temporal gap which corresponds to the time between two images $dt = 100\mu s$ to have a maximum image displacement of 7 to 8 pixels maximum. The thickness of the layer is an important parameter which in our case is 1.5mm.

For each measurement plane, 1000 pairs of stereoscopic PIV images were captured in the first

campaign with two high-resolution cameras. Each image of 16MP is captured at a frequency of 2Hz, with a time of 80μs between two consecutive images. The cameras have a Scheimpflug setup which enables them to work in conditions such that the object, the objective plane and the image plane have a common axis. This way the whole plane can be captured without having requiring a bigger lens aperture.

The software “DynamicStudio v4” developed by Dantec Dynamics is used for correlate these groups of four images (two of each camera), in order to find the velocity vectors of these particles and to determine the actual flow field. An overall view of the setup is shown in figure 6.

4 NUMERICAL APPROACH

The numerical calculations carried out in this project are computed by the CFD solver STARCCM+. The objective is to solve the URANS (unstationary RANS) incompressible equations using the gradient method (hybrid gauss-LSQ) which is an implicit unstationary discretisation schema by finite volumes of second order in time and space. The turbulence model used is the Spalart-Allmaras model which will be briefly explained in the following section.

Since the flow is incompressible, a segregated flow approach is used instead of a coupled flow approach which would take a much longer time. Also, since the flow is incompressible and isothermal, constant density applies which also saves time.

4.1 Boundary conditions

The appropriate boundary conditions must be defined in the limits of the domain defined in the calculations.

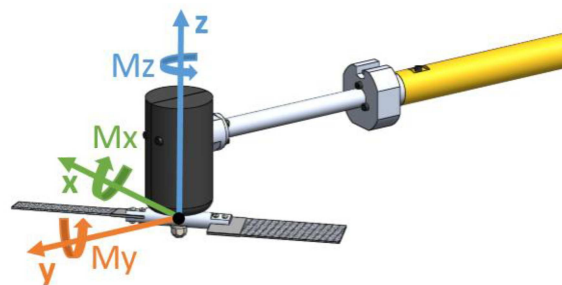


Figure 3 - Rotor frame of reference

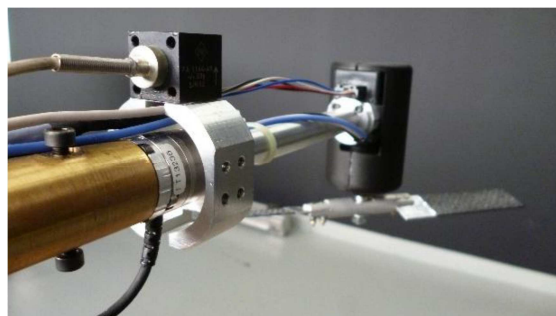


Figure 4 – Six-Component Force/Torque balance (ATI Nano 25)

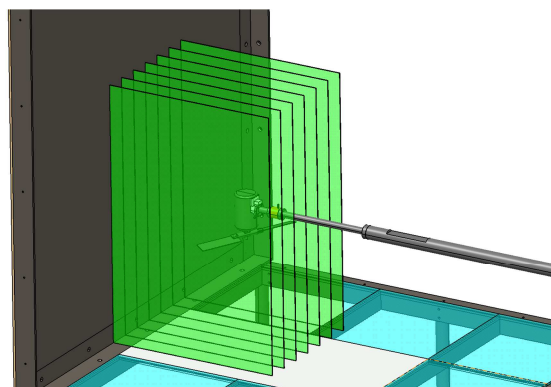


Figure 5 – PIV plane

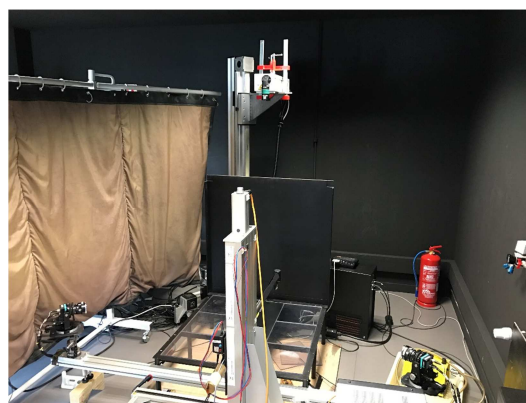


Figure 6 – PIV setup

In our three cases, different combinations of the following different boundary conditions were consequently imposed, [table 1](#):

- Stagnation inlet: far field condition in which the flow is at rest.
- Pressure outlet: defines the static pressure at the exit.
- Wall: represents an impermeable surface which separates the fluid and the solid medium. A slip condition is imposed.

4.2 Meshes

In the present case, the two blade rotor presented in previous sections has been reproduced with the exact same geometry. The two blades were designed using the software Gambit-ANSYS. Only the two blades of the rotor were created, without the hub, in order to actually analyse the aerodynamics of the blades without the influence of any other elements. The mesh around the blades is also created in Gambit. This mesh, called 3D-“O-Grid Mesh”, contains cells starting at 45° in any direction from the blade surface with face sizes of 1-2mm² in the first layers of the boundary layer mesh. Each one of these meshes will constitute an individual fluid region which will be rotating together with the blades. This region contains around 920,000 cells and its dimensions are 125mm in length and 25 by 50mm in the chord plane.

The mesh of the fluid volume was created separately in StarCCM+®, a CD Adapco® commercial CFD solver. This mesh is generated using a trimmer meshing technique. This method allows to create high-quality meshes for simple or complex geometries, using hexahedral cells.

Once both volumes have been meshed, the mesh around the blades and then blades are imported into StarCCM+®, [figure 7](#), [figure 8](#).

It is crucial to pay attention to the size ratio between the mesh around the blades and the

domain mesh. Where the two meshes are in contact the size of both must be very similar. Therefore, the mesh near the rotating volume will be 1mm and will grow progressively to reach a size of 5 mm within the domain.

Conditions	OGE	IGE	ILOCE
<i>Inlet</i>	Stagnation inlet	Stagnation inlet	Stagnation inlet
<i>Outlet</i>	Pressure outlet	Wall	Wall
<i>Laterals</i>	Pressure outlet	Pressure outlet	3 Pressure outlets + 1 wall

Table 1 – Boundary conditions for different study cases

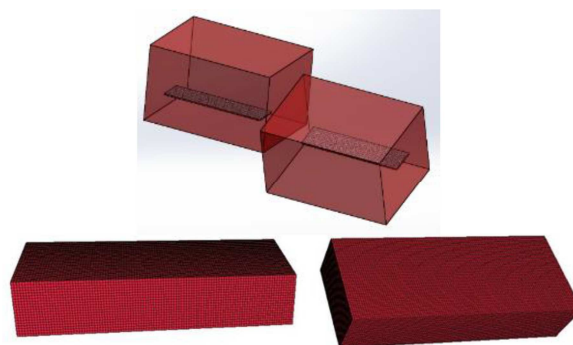


Figure 7 - Blade's Region mesh in CFD simulations

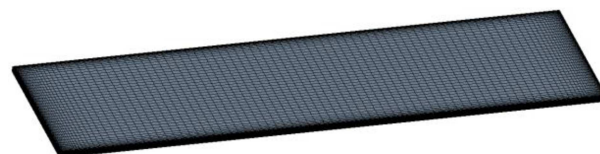


Figure 8 - Blade surface mesh

The trimmer mesh of the external region and the O-grid rotating mesh of the blade's region should be connected to allow the fluid exchange between both regions. This connection is carried out using the “Chimera Grid Method” or “Overlap Method”, which is known as Overset in StarCCM+®, which makes it possible to overlap two structured meshes enhancing the local resolution of the meshes. A continuous interpolation from one mesh to the other is done at each time step.

The control volume used for the OGE and IGE cases has a size of 250x500x250 mm. For the OGE case, the rotor is placed at a distance of one radius below the horizontal upper wall which corresponds to the stagnation inlet limit condition and at a distance of four radius of the lower wall which corresponds to the pressure outlet limit condition. In the IGE configurations the lower and upper walls are positioned at the different desired simulation distances.

To ensure the convergence, before our meshes were chosen, calculations were carried out with a finer and a coarser mesh size as well as with a shorter and a longer time step. Every rotor turn is divided into 180 time steps and each time step has 20 iterations. Each simulation has been carried out until 100 rotor turns were reached in the ILoCE cases and 50 rotor turns in the IGE cases. For each case, the convergence of the calculations has been checked by looking at the values of the blade forces reached throughout the simulations. Making a convergence test of this type is crucial in any numerical simulation as a non-converged simulation could lead to erroneous results, [figure 9](#).

5 RESULTS

5.1 Lift Values

As previously explained, to ensure that the results correspond to a constant lift value of 2N, the rotation speed for each case was found experimentally, this value was imposed in the numerical simulations and the results obtained were compared to those obtained experimentally. These results are shown in this sections and the proximity of both approaches can be remarked, [table 2 & 3](#).

It can be observed that the numerical approach tends to underestimate the lift value as most of the experimental lift values are below 2N. Unfortunately, a technical problem regarding the balance described in the experimental section

took place right after the RPM measurement for the ILoCE $h/R=2$ $d/R=2$ was recorded. Therefore this RPM was imposed in the rest of the ILoCE cases and it was checked in that the lift remained very close to the desired 2N in the numerical simulations. This RPM had a value of 4041.

5.2 Force distribution on blades

IGE case

In this section the lift and drag distributions along the blade is examined through the numerical approach in order to understand its behaviour in relation with the rotor's distance from the ground and/or wall. To obtain a constant lift value of approximately 2N, the values from experimental measurements had been used to find the rotation speed required to achieve the desired lift. This speed is then used in StarCCM+ where it is not possible to enter the lift directly. This means that the area under each mean lift graph is always approximately 2N if both blades are considered. The [figure 10](#) obtained by calculating the mean forces on the last turn after 50 rotor turns had been reached to ensure convergence. The reference case is the OGE and as expected, the closer the rotor is placed to the ground the more observable its influence becomes on the blade force distribution. Similarly, the IGE $h/R=2$ force distribution is extremely close to that of the OGE case.

Also, while the lift at $\frac{3}{4}$ blade span from the $h/R=1$ has a small change from the $h/R=0.5$, the change near the hub is very noticeable. The $h/R=0.25$ and the $h/R=0.5$ cases are far from the rest of the curves at $\frac{3}{4}$ blade span but similar to one another. Additionally, it is important to observe how the closer the rotor is to the ground the smaller the mean lift on the $\frac{3}{4}$ blade span is. The opposite is true as we approach the centre of the rotor. Therefore, it can be affirmed that the closer the rotor is to the ground the more uniform the mean lift distribution becomes. The same observations are true for the mean drag distributions.

IloCE case

Figure 11 clarifies some aspects of the results that will be presented in this section. Firstly, that a rotation begins with the rotor perpendicular to the wall and that we call blade 1 the blade that is closest to the wall in this position. Secondly, that the rotation is anticlockwise and the angle of rotation is measured as shown in the diagram above. In the case of the IloCE case figures 12 show that the total lift and drag values of blade 1 decrease as the blade moves away from its initial position perpendicular to the wall until it reaches a position parallel to the wall where the force increases again. This means of course, that simultaneously, the forces on blade 2 increase because a total 2N global lift force is achieved. It can be observed that the effect is most noticeable at $\frac{3}{4}$ of the blade since the forces at the tip and near the hub remain practically constant. The corner effect can also be represented as shown in figure 13 which shows the force distribution as seen from above for different rotor radius. The nonsymmetrical effect caused by the presence of the wall can be observed only for the larger radius numbers. Similarly, this effect can be observed in the force colour maps in figures 14 where it can be observed that the dissymmetry on each blade is the opposite than in the other one.

5.3 Wake

Although the analysis of the fluid flow doesn't lead to a direct quantification of the effects seen by the rotor it results in understanding of the physical phenomena that occurs and it helps us visualise the fluid-structure interaction directly. In this section, diagrams of iso-velocity in a plane section will be shown with the third velocity component represented with colour as to obtain a three-dimensional representation of the flow. The topology of the flows will be commented and

compared and in the case of IloCE the PIV results will also be presented.

OGE case

The reference case, the OGE, figure 15 shows us a perfectly symmetrical flow as expected. The transverse velocity shows us the anticlockwise rotation of the rotor with fluid coming in the plane at the right and out the plane at the left.

IGE case

The four IGE cases show how the fluid wake is deformed by the presence of the ground. For example for case $h/R=2$, figure 16. The effect is less visible as the rotor moves away from the ground and the IGE $h/R=2$ case shows that the effect of the ground right under the rotor is almost inexistent. However the other cases show how the jet is squashed due to the presence of the ground and how the flow recirculates upward and meets the rotor from underneath. It is important to remember the fact that the hub has not been simulated which means that some figures show the flow passing upwards in between the blades which is something that would not occur in a real rotor with a blade hub.

ILCoE case

In figure 17 left, we can observe the topology of the fluid wake in corner effect. A toroid can be observed in the blade hub area because the fluid goes into the plane at the right of the hub and out of the plane in the left. Clearly in this case the flow is not symmetrical. Two vortices can be observed underneath the rotor and a source or drain point is formed due to the wall. The interaction with the wall also causes this vortex to rise above the rotor and to interact with it form above. Similarly, figure 17 right shows the same figure with the results obtained from PIV. It can be observed that the PIV captured the same drain/source near the wall and the way that the vortex rises above the rotor. However, the vortices near the ground do not appear. This is because with 1000 PIV acquisitions convergence

of velocity derivatives is reached in almost all the region but it not reached near the masked part and the wall and ground. Therefore, a second PIV has been started with the objective of reaching 2500 acquisitions and allowing a more accurate study of the flow.

Another useful way to analyse the flow and the effect of the walls is to analyse the velocity profiles. The effect of the wall and ground is particularly noticeable as we approach the corner. The boundary layer of the ground and of the wall can also be observed and it resembles a flat jet boundary layer so the it could be interesting to further investigate the similarities between both.

6 CONCLUSION AND FUTURE WORK

Due to their small dimensions and versatility, drones are can be designed to perform missions in confined environments. Many sectors, such as archeology and nuclear security could greatly benefit from these developments. A way to enhance flight robustness is to understand how the rotor of a hovering drone responds to wall proximity in terms of its effect on the flow field, the force distribution it perceived and its aerodynamics performances. These three effects have been studied in this work and the physical link between them has begun to be analyzed to improve the physical understanding of confined flight.

It is important to understand that the work presented in this report is part of a bigger project were a lot of work has already been done and that there are still many options to investigate further. However, with this work we are one step closer to the final objective of designing and controlling drones flying in enclosed environments.

As it has been mentioned in the results rection, another PIV campaign is being carried out to reach more accurate experimental results. Also new numerical simulations have already been launched for other corner configurations. The idea

is to study the corner effect in us much detail as the ground effect.

Additionally, the other configurations mentioned in the geometry and configurations section such as the wall efect and the channel effect will also be researched to understand as many configurations as possible to be able to eventually fly drones in real enclosed environments. These configurations will continue to be analysed both numerically and experimentally. The PIV configuration will probably be changed to allow a more complete analysis of the fluid plane and the balance which had a problem will be recalibrated or replaced.

Another possible future step would be to move on from the static flight analysis and analyse the effect of different obstacles on a rotor carrying out dynamic flight. This could be done experimentally by replacing the displacement rod described in the experimental setup section by a robotic arm which would move the drone as commanded.

REFERENCES

- [1] A. Betz. The ground effect on lifting propellers. NACA TM 836, NACA.
- [2] Knight M. et Hefner R.A. Static thrust analysis of the lifting airscrew. Annalen der Physik, No. 626, 1937.
- [3] Knight M. et Hefner R.A. Analysis of ground effect on the lifting airscrew. National Advisory Committee for Aero.
- [4] Zbrozek J. Ground effect on the lifting rotor. Aeronautical Research Council, R M 2347, Juillet 1947.
- [5] Cheeseman I.C. et Bennett W.E. The effect of the ground on a helicopter rotor in forward flight. Aeronautical Research Council, R M 3021, 1957.
- [6] Hayden J.S. The effect of the ground on helicopter hovering power required. 32nd Annual

Forum of the American Helicopter Society, Washington D.C, Mai 1976.

[7] M.R Ritter. CFD analyses of the ground effect and the propulsion system of the BR2C micro drone. PhD thesis, Technical University of Munich, September 2008.

[8] V.K. Lakshminarayan et J.D. Baeder T.S Kalra. Cfd validation of micro hovering rotor in ground ef effect.

[9] V.J. Rossow. Thrust changes induced by ground and ceiling planes on a rotor in hover.

[10] H. Chung et K. Ryan D.C. Robinson. Computational investigation of micro rotorcraft near-wall hovering aerodynamics. International Conference on Unmanned Aircraft Systems (ICUAS), May 27-30 2014.

[11] C. Phillips. Computational Study of Rotorcraft Aerodynamics in Ground Effect and Brownout. PhD thesis, University of Glasgow, Mai 2010.

[12] N.D. Nathan. The Rotor Wake in Ground Effect and its Investigation in a Wind Tunnel. PhD thesis, University of Glasgow, Mai 2010.

[13] V.J. Rossow. Effect of ground and/or ceiling planes on thrust of rotors in hover. NASA Technical Memorandum 86754, Juillet 1985.

[14] Cristian Garcia Magana. Archean aerodynamics of rotor in confined environment. Institute for Space and Aeronautics, Juin 2015.

[15] V.K. Lakshminarayan. Computational Investigation of Micro-Scale Coaxial Rotor Aerodynamics in Hover. PhD thesis, University of Maryland, 2009.

[16] T. Jardin, S. Prothin, C. Garcia Magana. Aerodynamics of micro-rotors in confined environments. Journal of American Helicopter Society. Vol. 62, Number 2, pp. 1-7(7). 2017.

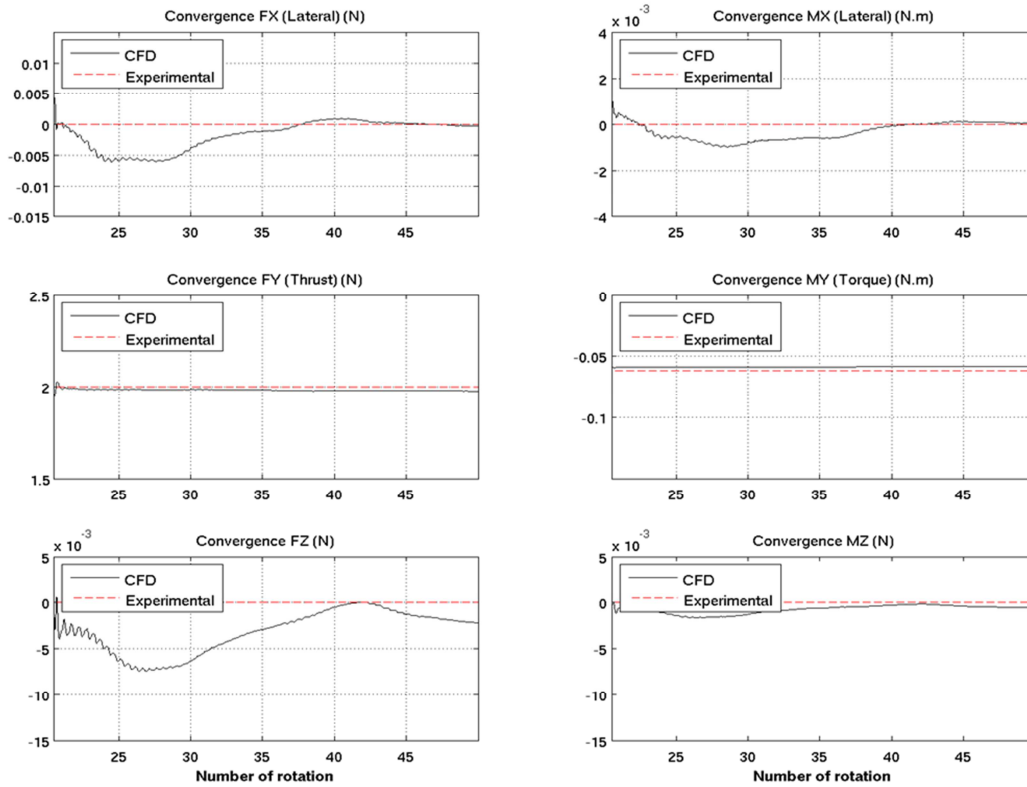


Figure 9 – Example of convergence in a simulation of a IGE case

OGE			
	Exp	Num	Ecart %
RPM	3810,7	3810,7	0
T (N)	2,000	1,869	7%
Q (N.m)	0,058	0,059	-2%
PL	0,087	0,080	8%

Table 2 – Numerical and experimental comparison in OGE

IGE												
h/R	RPM	T (N)			Q (N.m)			PL			Nb(num)	
		Exp	Num	Ecart %	Exp	Num	Ecart %	Exp	Num	Ecart %	Calculé	Exporté à partir
0,25	3324,7	2,00	2,052	-3%	0,052	0,053	-1%	0,110	0,112	-2%	50	40
0,5	3465,0	2,00	1,888	6%	0,051	0,052	-2%	0,108	0,100	7%	50	40
1	3765,8	2,00	1,990	1%	0,062	0,059	5%	0,082	0,086	-4%	50	40
2	3779,4	2,00	1,864	7%	0,057	0,058	-2%	0,089	0,082	8%	50	40

Table 3 – Numerical and experimental comparison in IGE

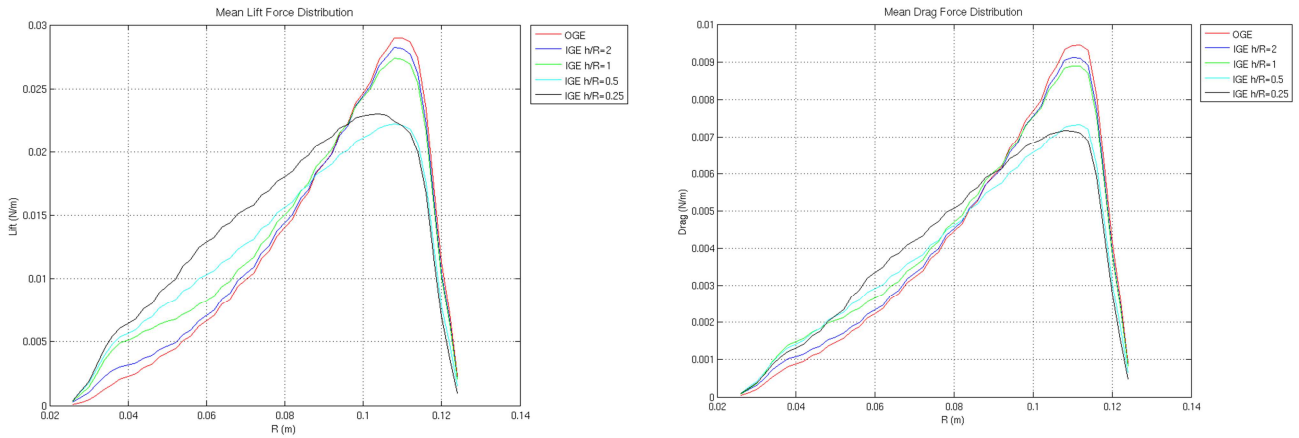


Figure 10 – Mean of lift/drag distribution for different IGE Cases (Numeical)

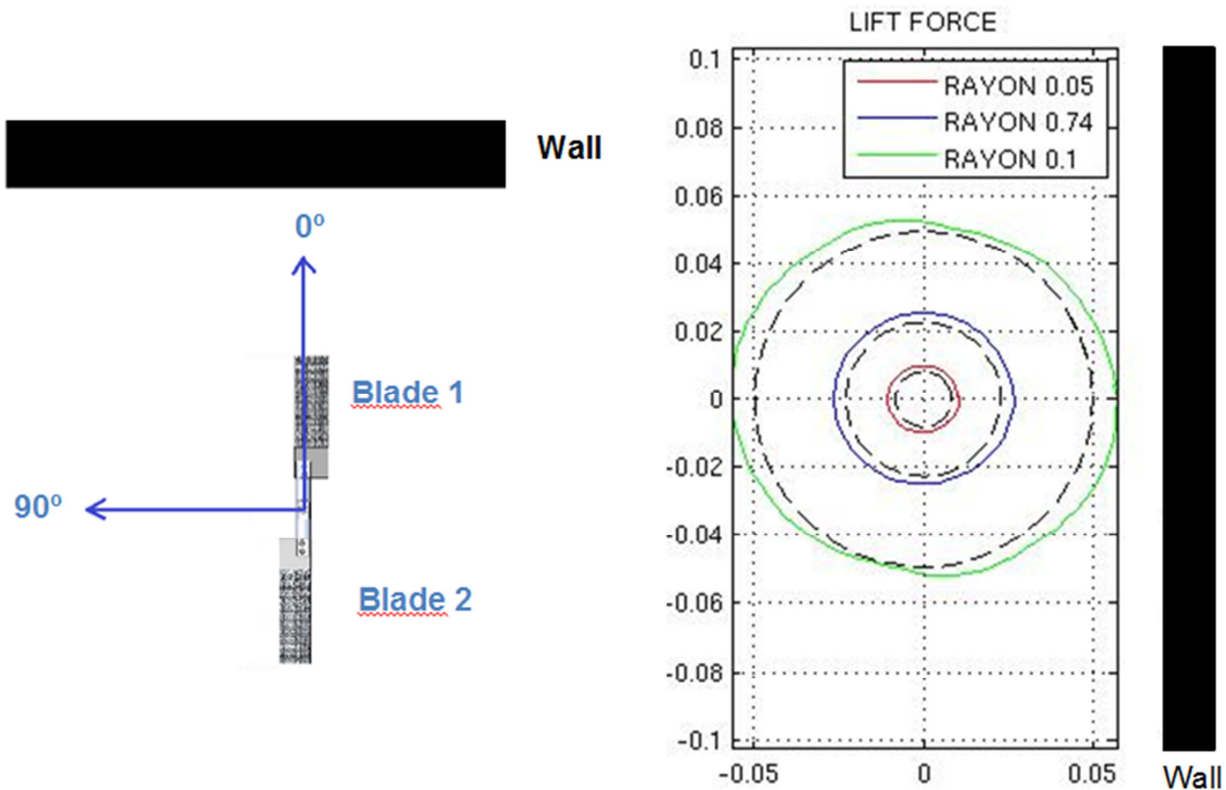


Figure 11 – ILoCE Diagram

Figure 13 – Lift Distribution ILoCE h/R=2 d/R=2 (Numerical)

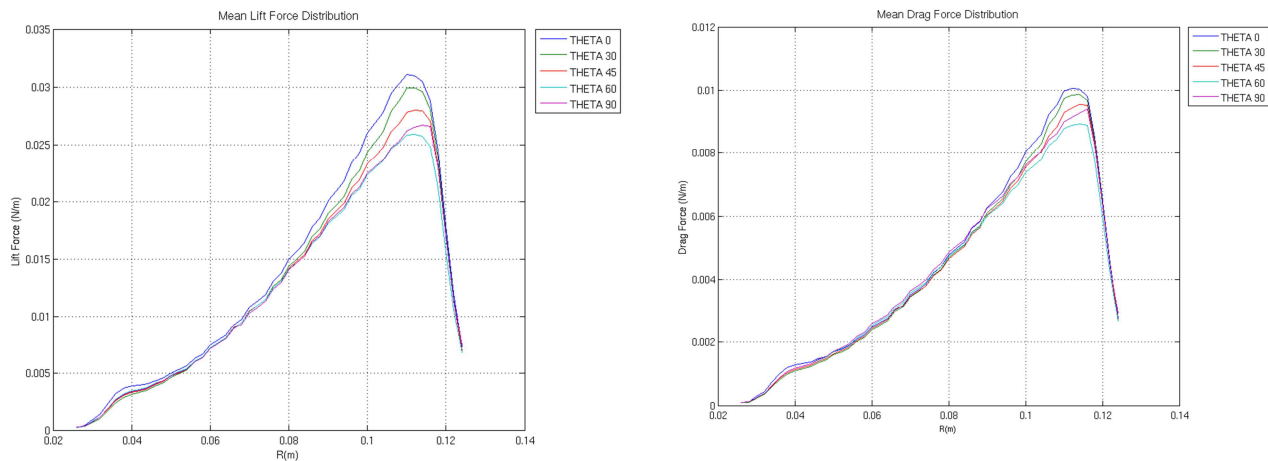


Figure 12 – Mean of lift/drag distribution for different ILoCE Cases (Numerical)

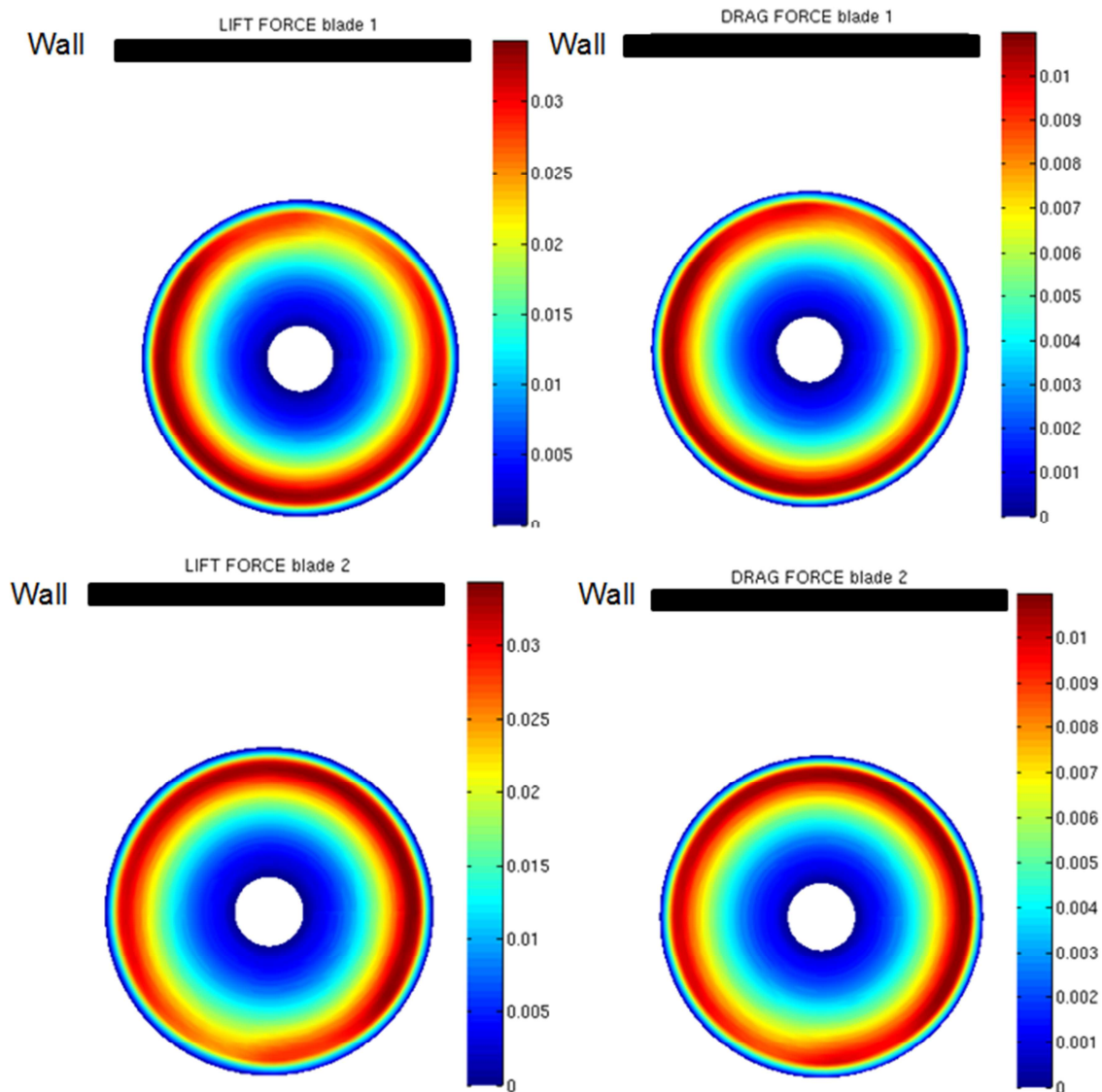


Figure 14 – Lift (left column) and Drag (Right column) force representation for the blade 1 (Upper Line) and blade 2 (lower line) (Numerical)

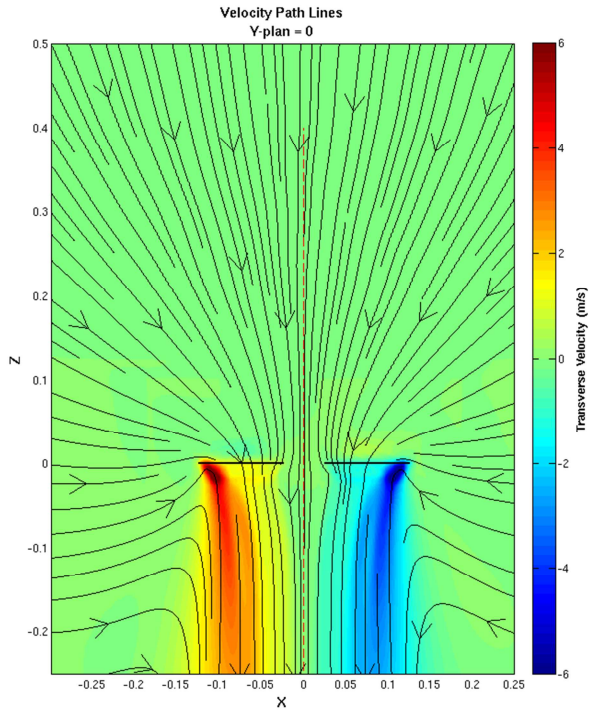


Figure 15 – Mean Velocity fields
OGE (Numerical)

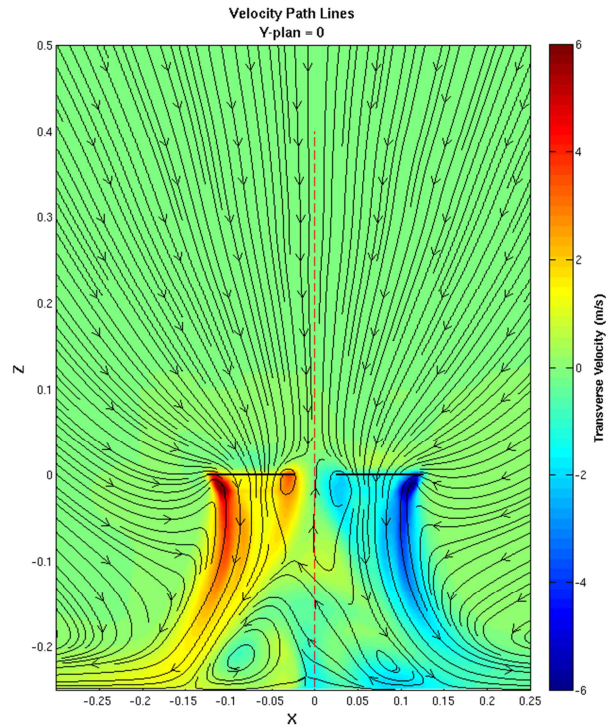


Figure 16 – Mean Velocity fields
IGE – $h/R = 2$ (Numerical)

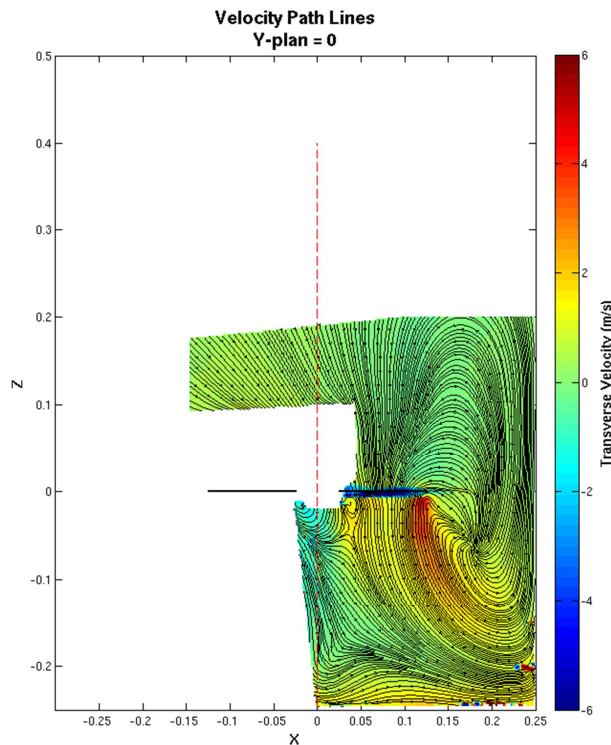
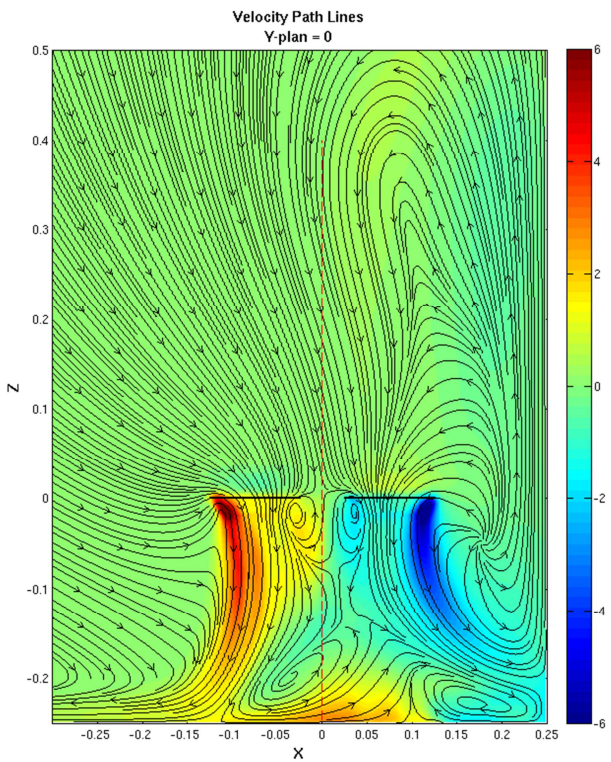


Figure 17 – Mean Velocity fields
ILoCE – $h/R = 2 - d/R = 2$
(Numerical : Left / Experimental : Right)